J|A|C|S
ARTICLES
Published on Web 03/20/2004

Oxygen Activation by the Noncoupled Binuclear Copper Site in Peptidylglycine α-Hydroxylating Monooxygenase. Reaction Mechanism and Role of the Noncoupled Nature of the Active Site

Peng Chen and Edward I. Solomon*

Contribution from the Department of Chemistry, Stanford University, Stanford, California 94305

Received December 6, 2003; E-mail: edward.solomon@stanford.edu

Abstract: Reaction thermodynamics and potential energy surfaces are calculated using density functional methods to investigate possible reactive Cu/O_2 species for H-atom abstraction in peptidylglycine α-hydroxylating monooxygenase (PHM), which has a noncoupled binuclear Cu active site. Two possible mononuclear Cu/O_2 species have been evaluated, the 2-electron reduced Cu^{II}_M-OOH intermediate and the 1-electron reduced side-on Cu^{II}_M-superoxo intermediate, which could form with comparable thermodynamics at the catalytic Cu_M site. The substrate H-atom abstraction reaction by the Cu^{II}_M-OOH intermediate is found to be thermodynamically accessible due to the contribution of the methionine ligand, but with a high activation barrier (~37 kcal/mol, at a 3.0-Å active site/substrate distance), arguing against the Cu^{II}_M-OOH species as the reactive Cu/O_2 intermediate in PHM. In contrast, H-atom abstraction from substrate by the side-on Cu^{II}_M-superoxo intermediate is a nearly isoenergetic process with a low reaction barrier at a comparable active site/substrate distance (~14 kcal/mol), suggesting that side-on Cu^{II}_M-superoxo is the reactive species in PHM. The differential reactivities of the Cu^{II}_M-OOH and Cu^{II}_M-superoxo species correlate to their different frontier molecular orbitals involved in the H-atom abstraction reaction. After the H-atom abstraction, a reasonable pathway for substrate hydroxylation involves a "water-assisted" direct OH transfer to the substrate radical, which generates a high-energy Cu^{II}_M-oxyl species. This provides the necessary driving force for intramolecular electron transfer from the Cu_H site to complete the reaction in PHM. The differential reactivity pattern between the Cu^{II}_M-OOH and Cu^{II}_M-superoxo intermediates provides insight into the role of the noncoupled nature of PHM and dopamine β-monooxygenase active sites, as compared to the coupled binuclear Cu active sites in hemocyanin, tyrosinase, and catechol oxidase, in O_2 activation.

1. Introduction

Cu proteins are common in biology and play important roles in O_2 activation and reduction.[1−3] Binuclear Cu proteins can be categorized into coupled or noncoupled Cu active sites based on the magnetic interaction between the two Cu^{II} centers.[4] Coupled binuclear Cu proteins include hemocyanin, tyrosinase, and catechol oxidase.[2] The two Cu centers at the active sites in these proteins are close in distance (~3.6 Å) and strongly antiferromagnetically coupled ($-2J \geq 1200\ cm^{-1}$, $H = -2JS_1 \cdot S_2$)[5] through bridging ligands, providing a direct mechanism for the 2-electron reduction of O_2 to form a peroxide-level intermediate species (side-on μ-η^2:η^2-$Cu_2(O_2)$), which is activated for electrophilic attack on substrates (in tyrosinase).[4] Noncoupled binuclear Cu proteins include peptidylglycine α-hydroxylating monooxygenase (PHM) and dopamine β-monooxygenase (Dβ M), both of which catalyze a substrate C−H bond hydroxylation (a glycine backbone C−H bond in PHM or a dopamine benzylic C−H bond in Dβ M) using molecular O_2 in a stereo- and regiospecific fashion.[3,4] The active sites of these two proteins consist of two inequivalent Cu centers largely separated in space (~11 Å in PHM)[6] with no direct bridging ligands and no observable magnetic interactions.[7] The crystal structure of PHM indicates that the Cu_M site (Figure 1A), where the substrate hydroxylation occurs, is coordinated by two histidine and one methionine ligands to the protein backbone, and the other Cu_H site (Figure 1B), which provides an additional electron through long-range electron transfer (ET) to the Cu_M site, has three histidine ligands from the protein.[3,6,8] Since the two Cu sites in PHM and Dβ M are noncoupled, the mechanism for this intramolecular long-range ET is not clear. A superoxide channeling mechanism[9] and a substrate-facilitated ET mechanism (either through the substrate[8] or through protein residues

(1) Holm, R. H.; Kennepohl, P.; Solomon, E. I. *Chem. Rev.* **1996**, *96*, 2239.
(2) Solomon, E. I.; Sundaram, U. M.; Machonkin, T. E. *Chem. Rev.* **1996**, *96*, 2563.
(3) Klinman, J. P. *Chem. Rev.* **1996**, *96*, 2541.
(4) Solomon, E. I.; Chen, P.; Metz, M.; Lee, S.-K.; Palmer, A. E. *Angew. Chem., Int. Ed.* **2001**, *40*, 4570.
(5) Tuczek, F.; Solomon, E. I. *Coord. Chem. Rev.* **2001**, *219−221*, 1075.
(6) Prigge, S. T.; Kolhekar, A. S.; Eipper, B. A.; Mains, R. E.; Amzel, L. M. *Science* **1997**, *278*, 1300.
(7) Ljones, T.; Skotland, T. In *Copper Proteins and Copper Enzymes*; Lontie, R., Ed.; CRC Press: Boca Raton, FL, 1984; p 131.
(8) Prigge, S. T.; Kolhekar, A. S.; Eipper, B. A.; Mains, R. E.; Amzel, L. M. *Nat. Struct. Biol.* **1999**, *6*, 976.
(9) Jaron, S.; Blackburn, N. J. *Biochemistry* **1999**, *38*, 15086.

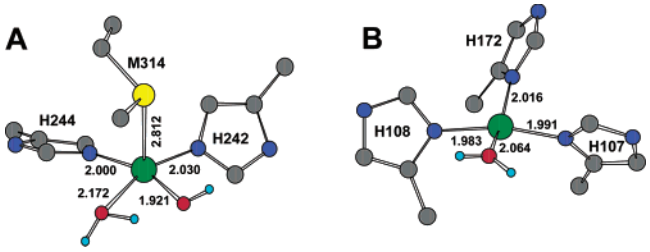

Figure 1. Optimized structures of oxidized Cu^{II}_M (A) and Cu^{II}_H (B).[22]

brought closer upon substrate binding[10]) have been proposed to account for this inter-Cu intramolecular ET process.

Previous kinetic and mechanistic studies have shown that the reaction mechanism for the substrate hydroxylation in PHM and DβM are very similar.[3] The enzymatic cycle starts with both the Cu_M and Cu_H sites at the Cu^I oxidation state (reduction by ascorbate in physiological conditions). When a substrate is present, O_2 reacts with the reduced protein forming a reactive Cu/O_2 intermediate, which then cleaves the substrate C−H bond via an H-atom abstraction mechanism generating a substrate radical.[11−14] Significant ^2H and ^{18}O isotope effects have been observed on the C−H bond cleavage reaction leading to the final hydroxylated product.[3,13,15−18] The reactive Cu/O_2 intermediate has been widely proposed to be an as-yet unobserved Cu^{II}−OOH species that would either abstract the substrate hydrogen directly or go through a Cu^{II}−oxyl intermediate first before abstracting the substrate H-atom (vide infra).[3] A Cu^{II}−O_2^{2-}/Cu^I−O_2^- species has also been proposed as a possible reactive intermediate for the H-atom abstraction reaction.[19]

Our previous studies on a mononuclear L3Cu^{II}−OOH complex (L3 = [HB(3-^{t}Bu-5-^{i}PrPz)$_3$], hydrotris(3-*tert*-butyl-5-isopropyl-1-pyrazolyl)borate) have shown that this hydroperoxo complex is not reactive for H-atom abstraction.[20] The peroxide σ^* orbital in this complex, which would be the acceptor orbital for H-atom abstraction, is high in energy and has only a small orbital coefficient on the terminal oxygen atom, indicating that it should be inefficient in H-atom abstraction. The product Cu^{II}−oxyl species that would be generated is also high in energy, resulting in a highly endothermic H−atom abstraction reaction by the L3Cu^{II}−OOH complex ($\Delta E \sim 45$ kcal/mol). We also studied a related Cu/O_2 species, a mononuclear side-on Cu^{II}−superoxo complex (L3$Cu^{II}O_2$),[21] which will also prove to be important in understanding oxygen activation at a single Cu center (vide infra). This L3$Cu^{II}O_2$ complex has a delocalized singlet ground state, which results from the highly covalent interaction between the Cu d_{xy} orbital and the superoxide π^*_σ orbital (the superoxide π^* orbital in the CuO_2 plane). The large covalency leads to high O_2 orbital coefficients in the ground-state LUMO, which is low in energy and may provide an efficient pathway for H-atom abstraction.

In another study,[22] we have spectroscopically and computationally defined detailed structural models for the oxidized Cu^{II}_M and Cu^{II}_H sites in resting PHM (Figure 1). The resting Cu^{II}_M site has a square pyramidal geometry with two His, one H_2O, and one OH^- as equatorial ligands and a Met as a long axial ligand. The resting Cu^{II}_H site has a slightly D_{2d} distorted square planar geometry with three His and one H_2O ligands. We further used N_3^- perturbation studies to provide a spectroscopic and electronic analogue to hydroperoxide binding to define the electronic structure of the putative Cu^{II}_M−OOH intermediate, which serves as a starting point for evaluation of energetics and mechanism of enzymatic substrate hydroxylation in PHM.[22]

In this study, we use the spectroscopically supported geometry optimized structures of Cu_M and Cu_H to computationally evaluate the possible reaction mechanisms of PHM. We start by evaluating the thermodynamics and energy barrier for the H-atom abstraction by the Cu^{II}_M−OOH intermediate, where the thermodynamics are improved by Met−S coordination to the Cu_M site relative to L3Cu^{II}−OOH. The Cu^{II}_M−OOH is not found to be reactive based on the high-energy barrier for H-atom abstraction. We then evaluate the alternative pathway involving a side-on Cu^{II}_M−superoxo intermediate. This pathway has favorable thermodynamics and a low energy barrier for the substrate H-atom abstraction. The Cu^{II}_M−OOH species produced is effective in hydroxylation of the substrate radical, resulting in a favorable intramolecular ET process (from Cu_H) to complete the enzymatic reaction. The differential reactivity pattern between the Cu^{II}_M−OOH and Cu^{II}_M−superoxo intermediates provides insights into the role of the noncoupled nature of PHM and DβM active sites, as compared to the coupled binuclear Cu active sites in O_2 activation.

2. Computational Details

Density functional calculations were performed on a PC cluster, using Gaussian 98.[23] All calculations were performed using the B3LYP functional[24] at the spin-unrestricted level. Geometry optimizations and frequencies were calculated with the LanL2Dz basis set. Single point energies and PCM solvation calculations were performed with the triple-ζ TZV basis set and tight SCF convergence on top of the optimized structures. Wave functions were visualized in Molden[25] and analyzed with AOMix.[26] Protein ligands were truncated to simplify the calculations. Methionines were modeled as ethyl methyl thioethers, and histidines were modeled as methylimidazoles. PHM crystal structures were taken as starting geometries, and the α-carbon positions were kept frozen during geometry optimizations. In some cases, these coordinate constraints result in one small imaginary frequency (~ -10 cm^{-1}) for

(10) Bell, J.; Meskini, R. E.; D′Amato, D.; Mains, R. E.; Eipper, B. A. *Biochemistry* **2003**, *42*, 7133.
(11) Fitzpatrick, P. F.; Flory, D. R.; Villafranca, J. J. *Biochemistry* **1985**, *24*, 2108.
(12) Fitzpatrick, P. F.; Villafranca, J. J. *J. Am. Chem. Soc.* **1985**, *107*, 5022.
(13) Miller, S. M.; Klinman, J. P. *Biochemistry* **1985**, *24*, 2114.
(14) Wimalasena, K.; May, S. W. *J. Am. Chem. Soc.* **1989**, *111*, 2729.
(15) Francisco, W. A.; Merkler, D. J.; Blackburn, N. J.; Klinman, J. P. *Biochemistry* **1998**, *37*, 8244.
(16) Francisco, W. A.; Knapp, M. J.; Blackburn, N. J.; Klinman, J. P. *J. Am. Chem. Soc.* **2002**, *124*, 8194.
(17) Francisco, W. A.; Blackburn, N. J.; Klinman, J. P. *Biochemistry* **2003**, *42*, 1813.
(18) Stewart, L. C.; Klinman, J. P. *Annu. Rev. Biochem.* **1988**, *57*, 551.
(19) Prigge, S. T.; Mains, R. E.; Eipper, B. A.; Amzel, L. M. *Cell. Mol. Life Sci.* **2000**, *57*, 1236.
(20) Chen, P.; Fujisawa, K.; Solomon, E. I. *J. Am. Chem. Soc.* **2000**, *122*, 10177.
(21) Chen, P.; Root, D. E.; Campochiaro, C.; Fujisawa, K.; Solomon, E. I. *J. Am. Chem. Soc.* **2003**, *125*, 466.
(22) Chen, P.; Bell, J.; Eipper, B. A.; Solomon, E. I. *Biochemistry*, in press.
(23) Frisch, M. J.; Trucks, G. W.; Schlegel, H. B.; Scuseria, G. E.; Robb, M. A.; Cheeseman, J. R.; Zakrzewski, V. G.; Montgomery, J. A., Jr.; Stratmann, R. E.; Burant, J. C.; Dapprich, S.; Millam, J. M.; Daniels, A. D.; Kudin, K. N.; Strain, M. C.; Farkas, O.; Tomasi, J.; Barone, V.; Cossi, M.; Cammi, R.; Mennucci, B.; Pomelli, C.; Adamo, C.; Clifford, S.; Ochterski, J.; Petersson, G. A.; Ayala, P. Y.; Cui, Q.; Morokuma, K.; Malick, D. K.; Rabuck, A. D.; Raghavachari, K.; Foresman, J. B.; Cioslowski, J.; Ortiz, J. V.; Stefanov, B. B.; Liu, G.; Liashenko, A.; Piskorz, P.; Komaromi, I.; Gomperts, R.; Martin, R. L.; Fox, D. J.; Keith, T.; Al-Laham, M. A.; Peng, C. Y.; Nanayakkara, A.; Gonzalez, C.; Challacombe, M.; Gill, P. M. W.; Johnson, B. G.; Chen, W.; Wong, M. W.; Andres, J. L.; Head-Gordon, M.; Replogle, E. S.; Pople, J. A. *Gaussian 98*, revision A.11.3; Gaussian, Inc.: Pittsburgh, PA, 1998.
(24) Becke, A. D. *J. Chem. Phys.* **1993**, *98*, 5648.
(25) Schaftenaar, G.; Noordik, J. H. *J. Comput.-Aided Mol. Des.* **2000**, *14*, 123.
(26) Gorelsky, S. I.; Lever, A. B. P. *AOMix program*; Revision 4.7 ed.; York University: Ontario, Canada, 2001.

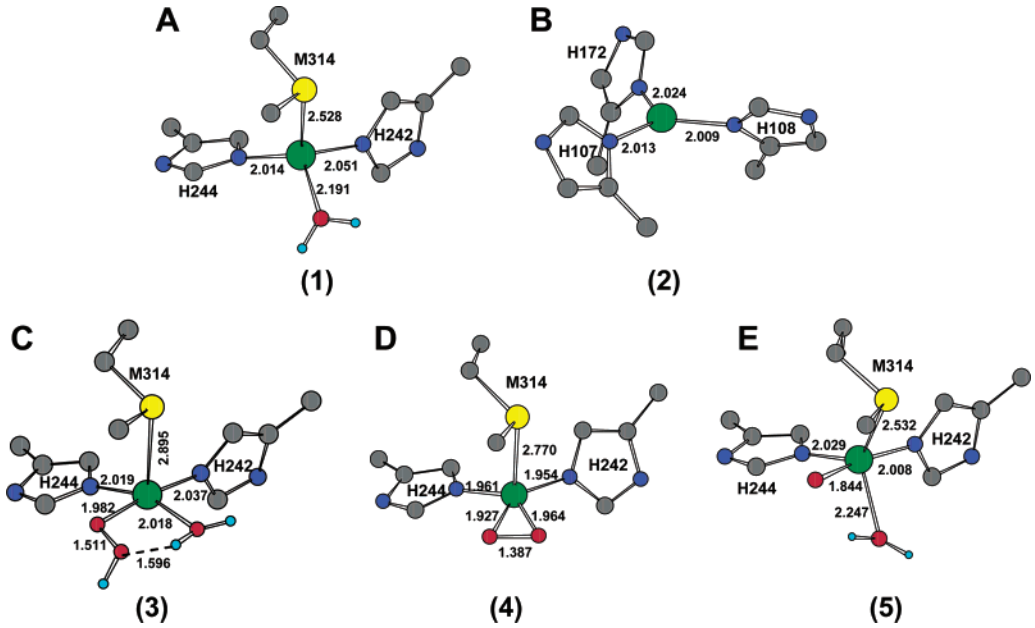

Figure 2. Energy optimized structures. Relevant bond lengths (Å) are indicated. (A) Reduced Cu^{I}_{M} site, $[Cu^{I}_{M}(Met)(His)_2(H_2O)]^+$. (B) Reduced Cu^{I}_{H} site, $[Cu^{I}_{H}(His)_3]^+$. (C) The putative hydroperoxo intermediate, $Cu^{II}_{M}-OOH$, $[Cu^{II}_{M}(Met)(His)_2(H_2O)(OOH)]^+$, from ref 22. (D) The side-on $Cu^{II}_{M}-$superoxo species, $[Cu^{II}_{M}(Met)(His)_2(O_2^-)]^+$. (E) The singlet $Cu^{II}_{M}-$oxyl species, $[Cu^{II}_{M}(Met)(His)_2(H_2O)(Oxyl)]^+$. Color codes: Cu, green; N, blue; C, gray; O, red; S, yellow; H, light blue.

the optimized structures with the corresponding vibrational modes involving mainly the motion of the α-carbons. In calculating the reaction coordinate, the geometries are considered converged when the total energy changes of subsequent geometry cycles are less than 1×10^{-6} hartree (~0.6 cal/mol). All reaction energetics were reported as changes in Gibbs free energies ΔG, unless otherwise noted, which includes zero point energies, thermal energies, entropies, and solvation energies (using dielectric constant $\epsilon = 5.0$ for the protein matrix). Solvation energies were also calculated with $\epsilon = 10$ and 20. No change was observed in the reaction energetics that would influence the conclusions of this study. Proton solvation energy in water was taken as −262.23 kcal/mol from a high-quality theoretical calculation using $(H_2O)_n$ clusters.[27] For reaction coordinate calculations, only changes in total electronic energies were calculated.

3. Results and Analysis

3.1. Cu Site Reduction and Formation of Reactive Cu/O_2 Species. 3.1.1. Reduced Cu^{I}_{M} and Cu^{I}_{H} Sites. The reduced Cu^{I}_{M} site was modeled with 1Met, 2His, and $1H_2O$ ligands and the reduced Cu^{I}_{H} site was modeled with 3His ligands. The energy optimized structures of reduced Cu^{I}_{M} and Cu^{I}_{H} sites are shown in Figure 2A and B ($[Cu^{I}_{M}(Met)(His)_2(H_2O)]^+$, **1**; $[Cu^{I}_{H}(His)_3]^+$, **2**). The Cu^{I}_{M} site has a tetrahedral geometry and the Cu^{I}_{H} site has a trigonal planar geometry, both consistent with the reduced structural models derived from XAS studies[28,29] and crystal structures. However, the geometries of the reduced sites Cu^{I}_{M} **1** and Cu^{I}_{H} **2** are different from the optimized structures of the oxidized Cu^{II}_{M} ($[Cu^{II}_{M}(Met)(His)_2(H_2O)(OH)]^+$) and Cu^{II}_{H} ($[Cu^{II}_{H}(His)_3(H_2O)]^{2+}$) sites (Figure 1A and B), which are square pyramidal and square planar, respectively.[22] The $Cu^{I}_{M}-$Met bond is ~2.53 Å, significantly shorter than that in the optimized structure of resting oxidized Cu^{II}_{M} (~2.81 Å, Figure 1A).[22] This shortening of the Cu−Met bond and significant geometry perturbations upon reduction of PHM (and DβM) have been observed experimentally in previous EXAFS studies.[28,30−32] The shortening of the Cu−Met bond on reduction is interesting and derives from the loss of the hydroxide ligand, which is a strong donor at the oxidized Cu^{II}_{M} site.[22] Upon reduction, the Cu_H site loses the bound water ligand and changes from the oxidized four-coordinate square planar structure to the reduced three-coordinate trigonal planar geometry.

3.1.2. Thermodynamics of the O_2 Reaction at Cu^{I}_{M} site. In reduced PHM, the two Cu centers (Cu_M and Cu_H) have potentially two electrons available for the O_2 reaction. Thus, both 2-electron and 1-electron reduction of O_2 are possible. With the accompanying oxidation of the reduced Cu^{I}_{H} site **2** (Figure 2B) to the resting oxidized Cu^{II}_{H} site[22] and protonation, O_2 reaction at the reduced catalytic Cu^{I}_{M} site **1** (Figure 2A) can generate the putative $Cu^{II}_{M}-OOH$ intermediate **3** (Figure 2C).[22] This reaction is endogonic by ~18 kcal/mol (Scheme 1A).[33] Alternatively, 1-electron reduction of O_2 by the reduced Cu^{I}_{M} site can generate a superoxide level intermediate without the second electron from Cu^{I}_{H} (Scheme 1B). The energy optimized structure of this $Cu^{II}_{M}-$superoxo intermediate is shown in Figure 2D (**4**, $[Cu^{II}_{M}(Met)(His)_2(O_2^-)]^+$). The bound water ligand of

(27) Tawa, G. J.; Topol, I. A.; Burt, S. K.; Caldwell, R. A.; Rashin, A. A. *J. Chem. Phys.* **1998**, *109*, 4852.
(28) Blackburn, N. J.; Rhames, F. C.; Ralle, M.; Jaron, S. *J. Biol. Inorg. Chem.* **2000**, *5*, 341.
(29) The bond lengths in the geometry optimized structures presented here are slightly longer than those determined experimentally. This is due to the basis set (LanL2Dz) employed in the geometry optimizations. The reaction energies calculated with the triple-ζ TZV basis set are not significantly affected by these small geometry differences. See: Szilagyi, R. K.; Metz, M.; Solomon, E. I. *J. Phys. Chem.* A **2002**, *106*, 2994. Schenk, G.; Pau, M. Y. M.; Solomon, E. I. *J. Am. Chem. Soc.* **2004**, *126*, 505.
(30) Boswell, J. S.; Reedy, B. J.; Kulathila, R.; Merkler, D. J.; Blackburn, N. J. *Biochemistry* **1996**, *35*, 12241.
(31) Scott, R. A.; Sullivan, R. J.; DeWolf, W. E., Jr.; Dolle, R. E.; Kruse, L. I. *Biochemistry* **1988**, *27*, 5411.
(32) Blackburn, N. J.; Hasnain, S. S.; Pettingill, T. M.; Strange, R. W. *J. Biol. Chem.* **1991**, *266*, 23120.
(33) Without protonation, this reaction is highly unfavorable (ΔG ~50 kcal/mol). The optimized structure of the generated species is best described as a $Cu^{I}_{M}-$superoxide rather than a $Cu^{II}_{M}-$peroxide species (data not shown). This species was also proposed as a possible reactive Cu/O_2 intermediate for H-atom abstraction from the substrate. (Prigge, S. T.; Mains, R. E.; Eipper, B. A.; Amzel, L. M. *Cell. Mol. Life Sci.* **2000**, *57*, 1236.) Since the formation of this species is highly unfavorable, it is excluded from further evaluation.

Scheme 1. Possible Pathways and Thermodynamics of O_2 Reaction at the Cu^{I}_{M} Site and H-Atom Abstraction by the Reactive Cu_M/O_2 Species[a]

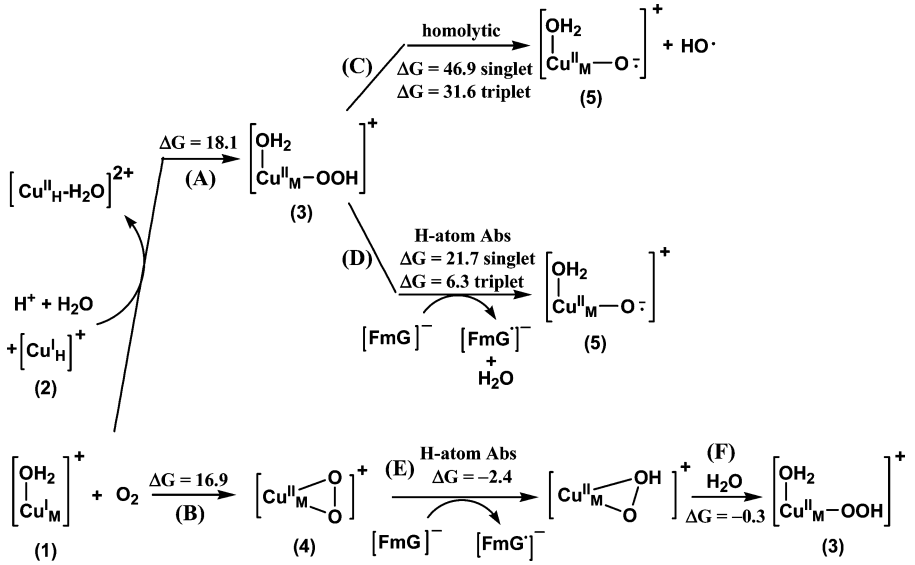

[a] Protein ligands are omitted for clarity in the scheme. All ΔG's are in kcal/mol. FmG, formylglycine.

the reduced Cu^{I}_{M} **1** is replaced by a superoxide moiety, which binds in a side-on fashion forming a square planar coordination geometry around the Cu center, very similar to the structure of the mononuclear side-on superoxide model complex $L3Cu^{II}O_2$ previously characterized.[21,29,34−36] The ΔG for forming this Cu^{II}_{M}−superoxo intermediate **4** is ∼17 kcal/mol,[35] comparable to that of the putative Cu^{II}_{M}−OOH intermediate **3** (Scheme 1A and B). Therefore, with comparable thermodynamics, O_2 reaction at the Cu_M site in the reduced PHM can generate two possible reactive Cu/O_2 intermediates, the 2-electron reduced peroxide level intermediate Cu^{II}_{M}−OOH **3** or the 1-electron reduced superoxide level intermediate Cu^{II}_{M}−superoxo **4**.

3.2. Cu^{II}_{M}−OOH Reaction Coordinate. 3.2.1. Reaction Thermodynamics. In PHM and DβM, the substrate C−H bond is cleaved via an H-atom abstraction mechanism.[11−14,37] In this section, we will evaluate the thermodynamics of the H-atom abstraction reaction on a peptide substrate with Cu^{II}_{M}−OOH **3** as the reactive intermediate. This possible reaction mechanism involves the homolytic cleavage of the peroxide O−O bond. A small substrate analogue formylglycine (FmG, $HCONHCH_2CO_2^-$) is used in calculating the thermodynamics. The energy optimized structure of FmG is given in Figure S1C (Supporting Information).

The thermodynamics of the homolytic cleavage of the O−O bond of the Cu^{II}_{M}−OOH intermediate, generating a singlet Cu^{II}_{M}−oxyl species (**5**, Figure 2E) and a HO• radical (Scheme 1C), is first evaluated as a reference. This reaction is highly unfavorable with ΔG ∼47 kcal/mol (ΔE ∼59 kcal/mol). The unfavorable thermodynamics of this O−O homolytic cleavage results from the high energy of the Cu^{II}_{M}−oxyl species generated, similar to the situation in the O−O homolytic cleavage of the $L3Cu^{II}OOH$ model complex.[20] However, the ΔE is ∼16 kcal/mol lower than that for $L3Cu^{II}OOH$ ($\Delta E_{\text{homolytic}}$ ∼75 kcal/mol),[20] which results from the contribution of the methionine ligand. The energy optimized structure of the singlet Cu^{II}_{M}−oxyl species **5** (Figure 2E) has a trigonal bipyramidal geometry with the oxyl atom and one histidine as the axial ligands. The methionine ligand is at an equatorial position and becomes partially oxidized relative to that in the Cu^{II}_{M}−OOH intermediate (Table S1, Supporting Information). Since the methionine sulfur is easier to oxidize than pyrazoles, which are partially oxidized in the $L3Cu^{II}$−oxyl product upon O−O homolytic cleavage of $L^3Cu^{II}OOH$,[20] the generated Cu^{II}_{M}−oxyl product species is relatively more stable. The overall reaction with Cu^{II}_{M}−OOH is still highly unfavorable. So far no experimental data are available on the spin state of any Cu^{II}−oxyl species. Therefore, the triplet state of the Cu^{II}_{M}−oxyl species was also calculated (Figure S1A, Supporting Information). The calculated triplet Cu^{II}_{M}−oxyl is lower in energy than the singlet state by ∼15 kcal/mol. This brings the thermodynamics of the Cu^{II}_{M}−OOH O−O homolytic cleavage to ΔG ∼32 kcal/mol (Scheme 1C), still an unfavorable reaction.

Direct H-atom abstraction on the FmG substrate by the Cu^{II}_{M}−OOH intermediate **3** leads to the additional formation of a O−H bond and cleavage of a substrate C−H bond relative to the O−O homolytic cleavage reaction (Scheme 1D), giving H_2O and the FmG• radical products (Figure S1D, Supporting

(34) Fujisawa, K.; Tanaka, M.; Moro-oka, Y.; Kitajima, N. *J. Am. Chem. Soc.* **1994**, *116*, 12079.

(35) Keeping the water ligand at the Cu_M site results in an end-on bound Cu^{II}−superoxide species with r_{O-O} ∼1.36 Å, r_{Cu-O} ∼1.95 Å, and ∠Cu−O−O ∼112° (Figure S2A, Supporting Information). This end-on Cu^{II}−superoxide species is ∼11 kcal/mol higher in free energy than the side-on Cu^{II}_{M}−superoxo species **4**. The H-atom abstraction by this end-on Cu^{II}−superoxide species to generate Cu^{II}_{M}−OOH **3** and the substrate radical is thermodynamically favorable with ΔG ∼−14 kcal/mol. The LUMO of this end-on Cu^{II}−superoxide species is the $(x^2-y^2)-\pi^*_\sigma$ orbital (Figure S2B, Supporting Information), which is slightly higher in energy (∼0.24 eV) than the LUMO of the side-on Cu^{II}_{M}−superoxide intermediate **4**. The MO coefficient of the terminal oxygen atom is ∼28%, slightly smaller than that of the side-on superoxide intermediate (∼32%, Figure 4B). From FMO theory, the energy barrier of the H-atom abstraction reaction by this end-on Cu^{II}−superoxide species should be at least as large as that for the side-on Cu^{II}_{M}−superoxide intermediate. Therefore, this end-on superoxide species is likely comparable to or slightly less reactive than the side-on superoxide species, not considering the steric effects of their different binding geometries.

(36) Note the reported crystal structure O−O bond length of this mononuclear side-on superoxide model complex $L3Cu^{II}O_2$ is underestimated due to the librational motion of bound O_2 unit at room temperature where the crystal structure was determined. (Cramer, C. J.; Tolman, W. B.; Theopold, K. H.; Rheingold, A. L. *Proc. Natl. Acad. Sci. U.S.A.* **2003**, *100*, 3635.)

(37) Zabriskie, T. M.; Cheng, H.; Vederas, J. C. *J. Am. Chem. Soc.* **1992**, *114*, 2270.

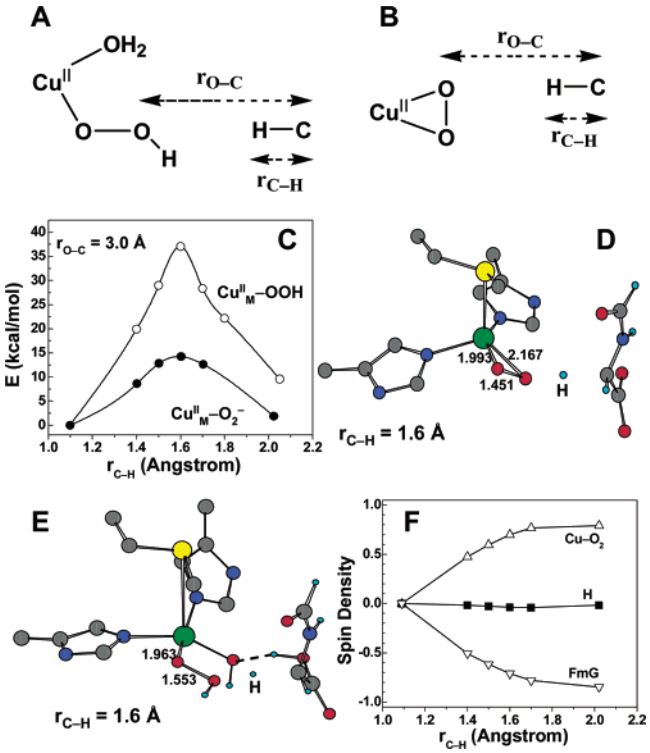

Figure 3. (A) Schematic representation of the H-atom abstraction reaction coordinate of Cu^{II}_M−OOH with substrate FmG. (B) Schematic representation of the H-atom abstraction reaction coordinate of Cu^{II}_M−superoxo with substrate FmG. (C) Calculated potential energy surfaces of H-atom abstraction reactions of Cu^{II}_M−OOH and Cu^{II}_M−superoxo with substrate FmG along the r_{C-H} coordinate at $r_{O-C} = 3.0$ Å. Energies are referenced to those of the reactants, which are set to zero. The reaction coordinates start at $r_{C-H} \sim 1.09$ Å, where the H-atom is bound at the substrate, and end at $r_{C-H} \sim 2.05$ Å, where the H atom is completely transferred. (D) The transition-state structure of H-atom abstraction reaction of Cu^{II}_M−superoxo with FmG. (E) The transition-state structure of H-atom abstraction of Cu^{II}_M−OOH with FmG. (F) Spin density changes on the CuO_2 moiety, the H being transferred, and the FmG moiety (transferred H not included) along the H-atom abstraction reaction coordinate of Cu^{II}_M−superoxo with FmG.

Information).[38] The O−H bond is strong and the C−H bond on the backbone carbon of glycine is additionally activated from resonance delocalization of the FmG• radical generated. The energy difference between the O−H and substrate C−H bonds thus produces additional driving force and brings the ΔG's of the H-atom abstraction reaction down to ~22 ($\Delta E \sim 37$ kcal/mol, singlet Cu^{II}_M−oxyl product) and ~6 kcal/mol ($\Delta E \sim 25$ kcal/mol, triplet Cu^{II}_M−oxyl product) (Scheme 1D). The low values of these ΔG's indicate that the H-atom abstraction by the Cu^{II}_M−OOH intermediate is in principle a possible pathway, dependent on the activation energy barrier of this reaction.

3.2.2. Energy Barrier for H-Atom Abstraction. To probe the possible barrier of the H-atom abstraction reaction by the Cu^{II}_M−OOH intermediate **3** (Figure 2C), the electronic potential energy surface (PES) was calculated along the H-atom transfer reaction coordinate as defined in Figure 3A. The position and orientation of the substrate analogue FmG relative to the Cu^{II}_M−OOH intermediate is estimated from the substrate-bound PHM crystal structure.[8] At one r_{O-C} distance, the H is moved toward the terminal oxygen atom of the Cu^{II}_M−OOH intermediate in steps by elongating the substrate C−H bond (r_{C-H}), while optimizing the rest of the geometric degrees of freedom at each step.[39] The calculated PES at $r_{O-C} = 3.0$ Å is shown in Figure 3C (open circles). The reaction coordinate starts at $r_{C-H} \sim 1.09$ Å, where the H is bound to the FmG substrate, and ends at $r_{C-H} \sim 2.05$ Å, where the H is completely transferred and the O−O is broken forming the H_2O product. The FmG moiety (excluding the transferred H) in the final product complex has a total spin density of ~ −1.0, indicating its radical nature and consistent with a net H-atom transfer reaction. The Cu^{II}_M−oxyl moiety in the product complex has a total spin density of ~2.0, indicating that it is in the triplet state. The energy difference between the product and reactant complexes is ~10 kcal/mol.[40] Importantly, the PES along the H-atom transfer reaction coordinate shows a large energy barrier ($E_{activation}$) of ~37 kcal/mol at $r_{C-H} \sim 1.6$ Å, making this reaction kinetically highly unlikely. The geometric structure at this transition state is shown in Figure 3E, in which the H-atom is located between the glycine backbone carbon and the terminal oxygen of the Cu^{II}_M−OOH intermediate whose O−O bond is not yet cleaved. Moving the substrate FmG closer to the Cu^{II}_M−OOH intermediate did not significantly lower the barrier ($E_{activation}$ ~34 kcal/mol at $r_{O-C} = 2.8$ Å, and $E_{activation}$ ~20 kcal/mol at $r_{O-C} = 2.6$ Å).[41] This high-energy barrier indicates that the Cu^{II}_M−OOH intermediate H-atom abstraction reaction is kinetically unfavorable as a possible reaction pathway in PHM, although the overall energetics indicate that it is thermodynamically plausible (section 3.2.1).

3.3. Cu^{II}_M−Superoxo Reaction Coordinate. 3.3.1. Thermodynamics and Energy Barrier for H-Atom Abstraction. The thermodynamics of the H-atom abstraction reaction on the substrate FmG was also calculated with the side-on Cu^{II}_M−superoxo **4** (Figure 2D) as the reactive intermediate (Scheme 1E). The thermodynamics of this reaction is almost thermal neutral, $\Delta G \sim -2$ kcal/mol ($\Delta E \sim 4$ kcal/mol), indicating that it is a thermodynamically favorable reaction pathway.[35] The generated product is an asymmetrically bound side-on Cu^{II}−hydroperoxo species (Figure S1B, Supporting Information), which can readily convert to the spectroscopically calibrated[22] Cu^{II}_M−OOH intermediate **3** by binding a water molecule ($\Delta G \sim -0.3$ kcal/mol, Scheme 1F).

The electronic PES along the Cu^{II}_M−superoxo H-atom abstraction reaction coordinate (defined in Figure 3B) was also calculated to probe the reaction energy barrier given in Figure 3C for $r_{O-C} = 3.0$ Å. At $r_{C-H} \sim 2.05$ Å, where the H is completely transferred to the Cu^{II}_M−superoxo intermediate, the substrate FmG moiety (excluding the transferred H) in the product complex has a total spin density of ~−0.85, reflecting its radical character and the net H-atom transfer reaction. The energy difference between the product and the reactant com-

(38) Another possible pathway of H-atom abstraction reaction by the Cu^{II}_M−OOH intermediate is to transfer the substrate H to the ligating O-atom generating the resting oxidized Cu^{II}_M site $[Cu^{II}_M(Met)(His)_2(H_2O)(OH)]^+$, the substrate FmG• radical, and a HO• radical ($\Delta G \sim 16$ kcal/mol). Because the ligating oxygen atom of the Cu^{II}_M−OOH intermediate is sterically inaccessible, it is a unlikely pathway.

(39) The positions of α-carbons of Met/His ligands were kept frozen during the optimizations. The orientation of the FmG substrate was also fixed by freezing the relative angles and dihedrals of all heavy atoms relative to the Met/His α-carbons, except for the two oxygen atoms of the carboxylate group, to reduce the computational cost. The constraints on the substrate FmG in the PES calculations should have a very small effect on the overall energetics because the constrained angles and dihedrals changed little in geometry optimizations of isolated molecules (Figure S1C−E, Supporting Information).

(40) The difference in ΔE between the PES calculations and the energetics calculations with isolated molecules is due to the slight geometry differences and different intermolecular interactions among the reactants and products.

(41) The activation energies at $r_{O-C} = 2.8$ and 2.6 Å were calculated by estimating the transition-state positions along the H-atom transfer coordinate (r_{C-H}) using the calculated PES at $r_{O-C} = 3.0$ Å.

Scheme 2. Possible Pathways and Thermodynamics of Hydroxylation Reaction[a]

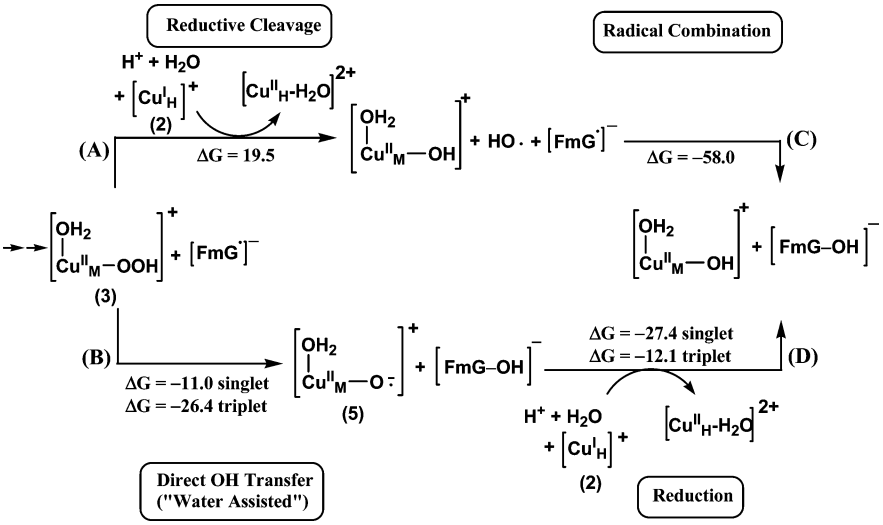

[a] Protein ligands are omitted for clarity in the scheme. All Δ*G*'s are in kcal/mol. FmG, formylglycine. FmG−OH, backbone C−H bond hydroxylated product of formylglycine.

plexes from the PES is ∼2 kcal/mol.[40] Importantly, the energy barrier at $r_{C-H} \sim 1.6$ Å along the H-atom transfer coordinate is only ∼14 kcal/mol, much lower than that for the Cu^{II}_M−OOH intermediate **3** (∼37 kcal/mol) at the same active site/substrate distance (Figure 3C). Moving the substrate FmG closer to the Cu^{II}_M−superoxo intermediate to r_{O-C} of 2.8 and 2.6 Å further decreases the energy barrier to ∼6 and ∼1 kcal/mol, respectively,[41] again much lower than the barriers for H-atom abstraction by the Cu^{II}_M−OOH intermediate at comparable active site/substrate distances (section 3.2.2). Together with the favorable reaction thermodynamics, the low-energy barrier indicates that the Cu^{II}_M−superoxo H-atom abstraction reaction is a highly favorable reaction pathway in PHM both thermodynamically and kinetically.[35]

The spin density changes on the CuO_2 fragment, the transferring H, and the FmG fragment (excluding the transferring H) are plotted in Figure 3F along the H-atom abstraction reaction coordinate. Continuous change in spin density on the CuO_2 and FmG fragments is observed, indicating that the electron of the net H-atom abstraction reaction is transferred continuously from the substrate to the Cu^{II}_M−superoxo intermediate. At the transition state ($r_{C-H} \sim 1.6$ Å), more than half the electron has been transferred. This is reflected in the O−O bond length (∼1.45 Å) of the transition-state structure shown in Figure 3D, which is significantly lengthened relative to that of the original Cu^{II}_M−superoxo intermediate (r_{O-O} ∼1.39 Å, Figure 2D), indicating the loss of superoxide and gain of peroxide character for the O_2 moiety along the reaction coordinate.

Interestingly, the transferring H does not have significant spin density at any step along the reaction coordinate (Figure 3F, solid squares) and is best described as a transferring proton. This indicates that the electron of the net H-atom abstraction reaction is transferred directly from the substrate to the Cu^{II}_M−superoxo intermediate and does not localize on the proton along the reaction coordinate. Therefore, this reaction is best described as a proton coupled electron transfer process (rather than H-atom abstraction), where the electron transfers through the superexchange pathway formed by the transferring proton via its covalent bonding interactions with the substrate backbone carbon and the oxygen atom of the $Cu^{II}M$−superoxo intermediate. This covalent bonding interaction is reflected in the small Mulliken charge of the transferring proton (+0.3), showing that while there is no spin density there is significant electron density on the proton. A similar proton coupled electron-transfer process was observed in the calculated reaction profile for the H-atom abstraction in lipoxygenases.[42] The continuous electron transfer and covalent superexchange pathway are both related to the significant overlaps between frontier molecular orbitals involved in the Cu^{II}_M−superoxo H-atom abstraction reaction, which will be discussed in section 4.2.

3.3.2. Hydroxylation of Substrate: Role of Intramolecular ET from Cu_H. The Cu^{II}_M−superoxo H-atom abstraction leads to the formation of the Cu^{II}_M−OOH intermediate **3** and the FmG• radical (Scheme 1E and F), which further hydroxylates the substrate, cleaves the O−O bond, and oxidizes the Cu^{I}_H site to complete the enzymatic reaction. Two possible reaction channels were evaluated: (1) O−O bond reductive cleavage followed by radical combination (Scheme 2A and C); (2) Direct OH transfer to the substrate followed by reduction of the generated Cu_M intermediate (Scheme 2B and D).

Reductive Cleavage plus Radical Combination. This possible channel starts with the intramolecular electron transfer from the reduced Cu^{I}_H site **2** (Figure 2B) to the Cu^{II}_M−OOH intermediate **3** (Figure 2C). This ET process would trigger the homolytic cleavage of the O−O (Reductive Cleavage), similar to the well-known Fenton reaction,[43] generating an HO• radical and a Cu^{II}_M−oxide species, which would rapidly protonate to produce the resting oxidized Cu^{II}_M site[22] (Scheme 2A). The HO• radical then combines with the FmG• radical forming the final hydroxylated FmG−OH product (Radical Combination, Scheme 2C, Figure S1E, Supporting Information). Although the second radical combination step is highly exergonic (Δ*G* ∼−58 kcal/mol), the first reductive cleavage step involving the Cu^{I}_H ET is endogonic by ∼20 kcal/mol. Thus, the barrier for this reductive cleavage reaction must be at least 20 kcal/mol. This makes the reductive cleavage followed by radical combination reaction

(42) Lehnert, N.; Solomon, E. I. *J. Biol. Inorg. Chem.* **2003**, *8*, 294.
(43) Sheldon, R. A.; Koch, J. K. *Metal-Catalyzed Oxidations of Organic Compounds*; Academic Press: New York, 1981.

Scheme 3. Summary of Overall Reaction Mechanism in PHM[a]

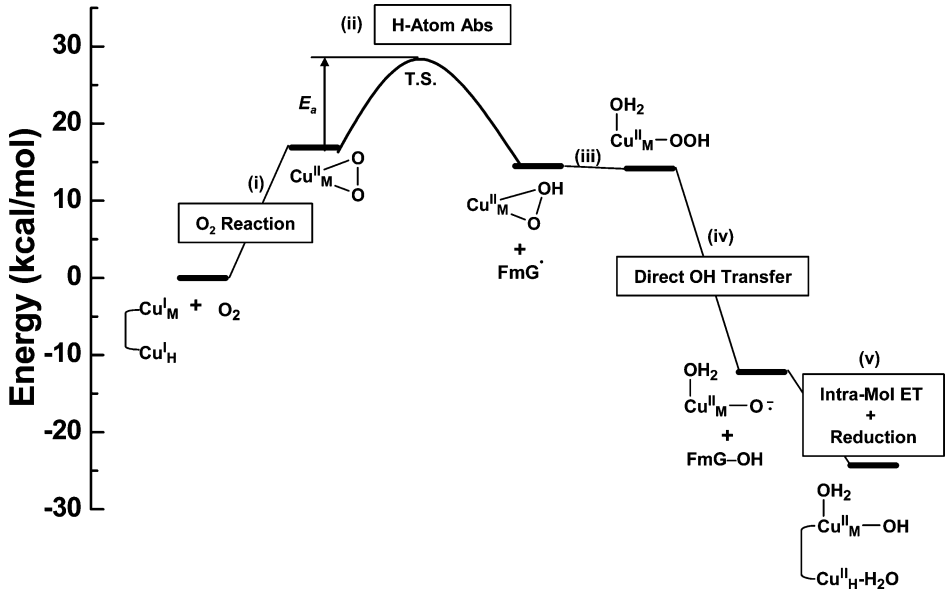

[a] For clarity, histidine and methionine ligands are omitted in the structures. Only species that are essential to the specified reaction are indicated on the scheme at each reaction step. See Scheme 1B, E, and F and Scheme 2B and D for details of each reaction step. Energies (free energy) are referenced to the initial reactants which are set to zero. T.S., transition state.

channel an unfavorable pathway for completing the hydroxylation reaction in PHM.

Direct OH Transfer plus Reduction. The second possible channel in Scheme 2B and D involves the initial direct transfer of the OH group from the Cu^{II}_M−OOH intermediate **3** to the FmG• radical forming the Cu^{II}_M−oxyl species **5** and the FmG−OH product (Direct OH Transfer, Scheme 2B, ΔG ∼−11(−26) kcal/mol for forming the singlet(triplet) Cu^{II}_M−oxyl species). The generated Cu^{II}_M−oxyl species **5** is then reduced by the Cu^{I}_H site **2** through an intramolecular ET to form the resting oxidized Cu^{II}_M site[22] (Reduction, Scheme 2D, ΔG ∼−27(−12) kcal/mol for the singlet(triplet) Cu^{II}_M−oxyl species). Both steps are exergonic and thus thermodynamically favorable.

The initial direct OH-transfer reaction (Scheme 2B) gains driving force by forming a strong C−O bond in the product FmG−OH, which compensates the energy cost in breaking the O−O bond of the Cu^{II}_M−OOH intermediate **3**,[44] and with a further contribution from the methionine ligand in stabilizing the Cu^{II}_M−oxyl species produced (see section 3.2). The OOH group of the Cu^{II}_M−OOH intermediate **3** binds in an end-on fashion due to the additional bound water ligand (relative to Cu^{II}_M−superoxo **4**) with the terminal O atom ∼2.92 Å away from the Cu center (Figure 2C), almost 1 Å longer than in the original side-on Cu^{II}_M−superoxo intermediate (Figure 2D, r_{Cu-O} ∼1.96 Å). This long $r_{Cu-O(H)}$ distance passes the OH group closer to the substrate radical after the H-atom abstraction reaction, facilitating OH group transfer. This suggests an interesting "water-assisted" OH transfer reaction mechanism that may be operative in the PHM reaction.

The final reduction reaction involves intramolecular ET from the Cu^{I}_H site and is also downhill in free energy (Scheme 2D), in contrast to the Cu^{I}_H ET reductive cleavage reaction in the reaction channel evaluated above (Scheme 2A, section 3.2.1). This is due to the high-energy nature of the Cu^{II}_M−oxyl species produced in Scheme 2B (see section 3.2.1). Reducing this Cu^{II}_M−oxyl species to the stable resting Cu^{II}_M state creates the necessary driving force to complete the reaction.

In summary, compared to the thermodynamically unfavorable reductive cleavage plus radical combination channel (Scheme 2A and C), the direct OH transfer plus reduction channel is a feasible reaction pathway for completing the substrate hydroxylation reaction in PHM. In this pathway, the initial O−O bond cleavage forms a high-energy species that provides the necessary driving force for reduction by intramolecular ET from the Cu^{I}_H site.

4. Discussion

Starting with the spectroscopically defined species in another study,[22] reaction thermodynamics and potential energy surfaces have been calculated by DFT methods to investigate possible reactive Cu/O_2 species for H-atom abstraction by PHM and the subsequent reaction channels, which complete the hydroxylation of substrate. Two possible mononuclear Cu/O_2 species have been evaluated, the 2-electron reduced Cu^{II}_M−OOH intermediate **3** (Figure 2C) and the 1-electron reduced side-on Cu^{II}_M−superoxo intermediate **4** (Figure 2D), which could form with comparable thermodynamics (ΔG ∼17−18 kcal/mol) at the catalytic Cu_M site of PHM (section 3.1). Although substrate H-atom abstraction by the Cu^{II}_M−OOH intermediate is possible with respect to the reaction thermodynamics, this reaction has a high activation barrier (∼37 kcal/mol), which argues against the Cu^{II}_M−OOH species as the reactive Cu/O_2 intermediate in PHM (section 3.2). In contrast, H-atom abstraction from substrate by the side-on Cu^{II}_M−superoxo intermediate is a nearly isoenergetic process with a low reaction barrier (∼14 kcal/mol) at a comparable active site/substrate distance (Scheme 3, step ii), which suggests that side-on Cu^{II}_M−superoxo may be the reactive species in PHM (section 3.3.1). Following the H-atom abstraction, a reasonable reaction pathway for substrate hydroxylation involves direct OH transfer (Scheme 3, step iv) and reduction by

(44) The ΔE for homolytic cleaving the C−O bond of FmG-OH is ∼79 kcal/mol, as compared to ∼59 kcal/mol for homolytic cleaving the O−O bond of the Cu^{II}_M−OOH intermediate **3**.

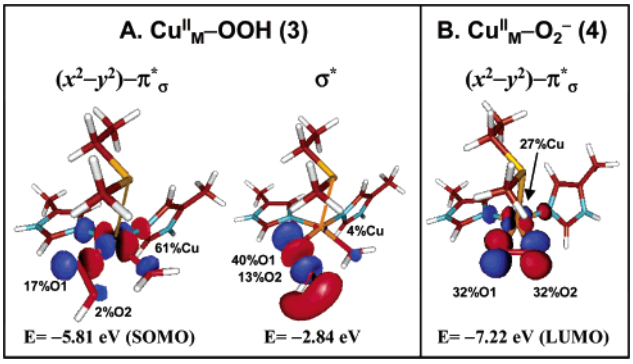

Figure 4. Surface contour plots of relevant frontier molecular orbitals of the Cu^{II}_M–OOH intermediate **3** (A) and the side-on Cu^{II}_M–superoxo intermediate **4** (B). Orbitals are named based on their main characters. Orbital decompositions (%) and energies (eV) are labeled. SOMO, singly occupied molecular orbital. LUMO, lowest unoccupied molecular orbital.

intramolecular ET from the Cu^I_H site (Scheme 3, step v, and section 3.3.2).

4.1. Relative Stability of the Cu^{II}_M–OOH and Cu^{II}_M–Superoxo Species. The calculations show that the 2-electron reduced Cu^{II}_M–OOH intermediate **3** and the 1-eletron reduced Cu^{II}_M–superoxo intermediate **4** from the O_2 reaction at the Cu^I_M site could form with comparable thermodynamics. This is somewhat surprising considering the large difference between the 2-electron and 1-electron reduction potentials of O_2 in H_2O, where the 2-electron reduction is much more favorable than the 1-electron reduction (at pH 7, $E°(O_2/H_2O_2) = 0.28$ V, $E°(O_2/O_2^-) = -0.33$ V versus NHE).[45] This suggests that the formation of the 2-electron reduced peroxo-level species Cu^{II}_M–OOH should be more thermodynamically favorable than the 1-electron reduced superoxo-level species Cu^{II}_M–superoxo. However, the side-on Cu^{II}_M–superoxo intermediate is stabilized by the formation of two covalent Cu–O bonds via a side-on binding mode (the calculated LUMO is very covalent and contains ~63% O_2 character, Figure 4B), while there is only one Cu–O bond formed in the Cu^{II}_M–OOH intermediate, which has low covalency (the calculated SOMO only contains ~19% O_2 character, Figure 4A). Experimentally, the Cu–O bond strength of the Cu^{II}_M–superoxo intermediate can be estimated from the Cu–O force constant (~2.20 mdyn/Å) of the structurally similar superoxo model complex $L3CuO_2$[21] and the fact that there are two Cu–O bonds in Cu^{II}_M–superoxo. The single Cu–O bond strength of the Cu^{II}_M–OOH intermediate should be weaker than that of the model complex $L3Cu^{II}$–OOH (~2.94 mdyn/Å),[20] because Cu^{II}_M–OOH has a less covalent Cu–O interaction.[22] Including the additional energy cost in oxidizing the Cu^I_H site in forming the Cu^{II}_M–OOH intermediate, the Cu^{II}_M–superoxo intermediate could thus form with thermodynamics comparable to the Cu^{II}_M–OOH species, even though the reduction potentials indicate that the 2-electron reduction of O_2 is highly favored.

4.2. Relative Effectiveness of H-Atom Abstraction. The calculated PESs along the H-atom transfer coordinate show that the side-on Cu^{II}_M–superoxo intermediate **4** is a much more effective Cu/O_2 species in H-atom abstraction reaction with a low activation energy barrier than the Cu^{II}_M–OOH intermediate **3** (Figure 3C, sections 3.2 and 3.3). These relative reactivities of the Cu^{II}_M–OOH and Cu^{II}_M–superoxo intermediates can be understood from their frontier molecular orbitals (FMO). In FMO theory,[46–49] large orbital coefficients (thus overlaps) and small energy separation of the interacting donor/acceptor orbitals lead to high reactivity. The FMO concept has been used previously in combination with electronic structure calculations to evaluate reactivity patterns of biologically relevant Cu_n/O_2 species.[4,50] The donor in the H-atom abstraction reaction is the C–H bond orbital. The Cu^{II}_M–OOH intermediate has two O_2-based unoccupied (or partially unoccupied) orbitals available as possible acceptors, the singly occupied molecular orbital (SOMO) $(x^2-y^2)-\pi^*_\sigma$ and the unoccupied orbital σ^* (Figure 4A). The $(x^2-y^2)-\pi^*_\sigma$ orbital has very little O_2 π^*_σ character on the terminal oxygen (~2%, Figure 4A, left) that would be available for attack on the substrate C–H bond and thus should not be an effective acceptor in H-atom abstraction. The σ^* orbital is ~3 eV higher in energy than the SOMO $(x^2-y^2)-\pi^*_\sigma$ and has dominant O_2 characters (53%, Figure 4A, right). However, the σ^* orbital is highly polarized toward the Cu due to protonation and only contains ~13% terminal oxygen character.[20,22] Alternatively, the LUMO of the Cu^{II}_M–superoxo intermediate is the $(x^2-y^2)-\pi^*_\sigma$ orbital, which is ~4.4 eV lower in energy than the σ^* orbital of the Cu^{II}_M–OOH intermediate and has large coefficients on the O_2 moiety (~32% on each oxygen, Figure 4B). The low energy of the Cu^{II}_M–superoxo $(x^2-y^2)-\pi^*_\sigma$ orbital reduces its energy separation from the C–H donor orbital that is deep in energy. The large orbital coefficient on the oxygen atom in the Cu^{II}_M–superoxo intermediate further gives better overlap with the donor C–H bond. Therefore, the Cu^{II}_M–superoxo intermediate should be a much more reactive Cu/O_2 species in H-atom abstraction relative to the Cu^{II}_M–OOH intermediate; this is reflected in the relative heights of the energy barriers in the calculated PESs (Figure 3C).

Looking at the transition-state structures, the transferring H-atom is located midway between the substrate and the Cu/O_2 species (Figure 3D and E). The C–H bond is broken but the O–H bond has not fully formed, which is energetically unfavorable and leads to the barrier in the reaction coordinate. The height of this barrier is dependent on how well the proton can overlap with the acceptor. Shorter active site/substrate distances could give better overlap between the acceptor orbitals of Cu/O_2 species and the substrate C–H bond and, thus, would lower the energy barrier for H-atom abstraction. The calculated barriers at shorter r_{O-C} distances show that the H-atom abstraction by the Cu^{II}_M–superoxo intermediate always has a much lower barrier than that for the Cu^{II}_M–OOH intermediate at comparable distances (sections 3.2.2 and 3.3.1), consistent with the Cu^{II}_M–superoxo species being more reactive in PHM.

4.3. Order of Hydroxylation and Cu_H ET. The Cu^{II}_M–superoxo H-atom abstraction reaction leads to the formation of the Cu^{II}_M–OOH intermediate and the substrate $FmG^•$ radical (Scheme 1E and F). The calculated reaction thermodynamics show that the favorable pathway involves the hydroxylation of the $FmG^•$ radical through a direct OH transfer reaction from the Cu^{II}_M–OOH intermediate followed by intramolecular ET

(45) Sawyer, D. T. *Oxygen Chemistry*; Oxford University Press: New York, 1991.
(46) Klopman, G. *J. Am. Chem. Soc.* **1968**, *90*, 223.
(47) Salem, L. *J. Am. Chem. Soc.* **1968**, *90*, 543.
(48) Salem, L. *J. Am. Chem. Soc.* **1968**, *90*, 553.
(49) Fleming, I. *Frontier Orbitals and Organic Chemical Reactions*; John Wiley & Sons: New York, 1976.
(50) Chen, P.; Solomon, E. I. *J. Inorg. Biochem.* **2002**, *88*, 368.

from the Cu^{I}_{H} site (Scheme 2B and D, section 3.3.2). This pathway results in a hydroxylation reaction that is thermodynamically downhill and generates the Cu^{II}_{M}−oxyl intermediate whose high reduction potential creates the driving force for the Cu^{I}_{H} ET. The implication of the need for this driving force for the intramolecular ET will be considered below.

4.4. Correlation to Experiments. Scheme 3 summarizes the PHM reaction mechanism with free energy correlations based on the calculated reaction thermodynamics and potential energy barriers. The outlined mechanism here is consistent with a number of reported experimental observations on the PHM reaction.[51] Klinman and co-workers reported ^{2}H (on the substrate C−H bond) and $^{18}O_2$ isotope effects on the reaction rate constant for the reactive Cu/O_2 species leading to the product,[15−17] which would include the reaction steps ii−v in Scheme 3. Reaction steps iv and v are strongly downhill, and reaction step iii is the simple, thermodynamically favorable water binding event, which likely has a very small or no energy barrier. Thus, the significant energy barrier of reaction step ii indicates that the H-atom abstraction reaction is most likely rate limiting in this reaction. This H-atom abstraction reaction involves the transfer of the substrate H-atom and significant bonding changes on one of the Cu bound oxygen atoms, which would be consistent with the observed ^{2}H and ^{18}O isotope effects. Significant H tunneling has also been reported.[16] Although the tunneling effect is not treated here, the substrate-bound PHM crystal structure[8] shows many H-bonding interactions between the substrate and protein residues that would bind the substrate at an appropriate distance from the Cu_M active site for H-tunneling through the energy barrier in Figure 3C and step ii in Scheme 3.[52]

The mechanism in Scheme 3 is also consistent with the fact that O_2 only reacts with reduced PHM with a substrate present.[3] Without substrates, this reaction would terminate at the Cu^{II}_{M}−superoxo intermediate stage (Scheme 3). Since the formation of the Cu^{II}_{M}−superoxo intermediate is uphill in free energy, the equilibrium is far to the left in Scheme 3 and no significant reaction should be observed. The fact that the methionine ligand has a much longer bond to the Cu center (and virtually no contribution to the ground-state wave function) in the oxidized Cu^{II}_{M} site than in the reduced Cu^{I}_{M} site indicates that methionine contributes to the stabilization of the reduced Cu_M site and keeps the O_2 binding reaction equilibrium far to the left. This would also explain the observation in DβM that no Cu^{II} EPR signal was detected after mixing the reduced protein with O_2 and an unreactive substrate analogue (C−H substituted with C−F).[3] The protein would mostly remain at the reduced state (i.e., Cu^{I}) with no EPR signal, and any Cu^{II}_{M}−superoxo intermediate formed would also not give a Cu^{II} EPR signal, since its ground state is a covalently delocalized singlet and is diamagnetic.[21]

4.5. Noncoupled versus Coupled Binuclear Cu Site Reactivity. As described in the Introduction, the Cu^{II} centers of the coupled binuclear sites in hemocyanin, tyrosinase, and

Chart 1. Possible Binuclear and Mononuclear Cu−O_2 Species

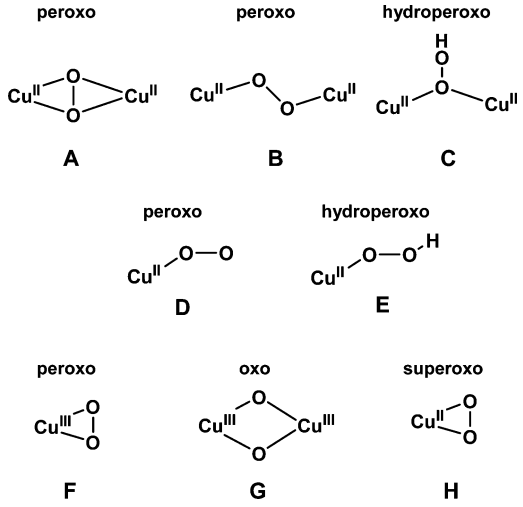

catechol oxidase are strongly coupled through a bridging ligand ($-2J \geq 1200\ cm^{-1}$),[5] which provides a direct mechanism for the 2-electron reduction of dioxygen generating a side-on bound $Cu_2(O_2^{2-})$ species (Chart 1A). The Cu centers of noncoupled binuclear sites (Cu_M and Cu_H) in PHM and DβM are distant from each other (∼11 Å in PHM),[6,8] with no observable magnetic interactions (i.e., very small J).[7] Since the catalytic reaction occurs at the Cu_M site and Cu_H acts only as a ET center,[3] an intramolecular ET process is necessary during the enzymatic reaction of PHM and DβM, whose rate is governed by Marcus theory (eq 1).[53] The ET rate constant k_{ET} is influenced

$$k_{ET} = \sqrt{\frac{\pi}{(h/2\pi)^2 \lambda k_B T}} (H_{DA})^2 \exp\left[-\frac{(\Delta G + \lambda)^2}{4\lambda k_B T} \right] \quad (1)$$

by the donor/acceptor electronic coupling matrix element (H_{DA}), the ET reaction driving force (ΔG), and the reorganization energy (λ), which includes the active site geometry change (λ_{inner}) and reorientation of the solvent dipoles (λ_{outer}, $\lambda = \lambda_{inner} + \lambda_{outer}$) associated with redox. The electronic coupling matrix element H_{DA} is connected to the exchange coupling constant J through eq 2, derived from a valence bond configuration

$$-2J = (H_{DA})^2/U \quad (2)$$

interaction model,[5,5454] where U is the metal−metal charge-transfer energy. Since the exchange coupling J is small for the noncoupled Cu_M and Cu_H sites, the $(H_{DA})^2$ must be small between the two Cu centers (eq 2). The significant geometry differences between the reduced and oxidized forms of the Cu_M and Cu_H sites also suggest that a large reorganization energy (λ_{inner}) is associated with the redox reaction of these two Cu sites. Therefore, to have a significant k_{ET}, there must be a large driving force ΔG for the ET process from Cu_H to Cu_M. The reaction mechanism in Scheme 3 indicates that PHM could achieve this through a direct OH transfer reaction to the substrate FmG• radical after the H-atom abstraction step (Scheme 3, step iv). The reduction and protonation of the high-energy Cu^{II}_{M}−oxyl species formed provides the necessary driving force for

(51) There are also other nonphysiological reactivities observed for DβM, in particular olefin epoxidation. (Padgette, S. R.; Wimalasena, K.; Herman, H. H.; Sirimanne, S. R.; May, S. W. *Biochemistry* **1985**, *24*, 5826.) This is also consistent with the Cu^{II}_{M}−superoxo pathway undergoing electrophilic attack. Epoxidation reactivities have been reported for some metal−superoxo species. See: Talsi, E. P.; Babenko, V. P.; Shubin, A. A.; Chinakov, V. D.; Nekipelov, V. M.; Zamaraev, K. I. *Inorg. Chem.* **1987**, *26*, 3871. Nakatsuji, H.; Hu, Z.-M.; Nakai, H.; Ikeda, K. *Surf. Sci.* **1997**, *387*, 328.

(52) Knapp, M. J.; Rickert, K.; Klinman, J. P. *J. Am. Chem. Soc.* **2002**, *124*, 3865.

(53) Marcus, R. A.; Sutin, N. *Biochim. Biophys. Acta* **1985**, *811*, 265.

(54) Brunold, T. C.; Gamelin, D. R.; Solomon, E. I. *J. Am. Chem. Soc.* **2000**, *122*, 8511.

the intramolecular ET from the Cu^{I}_{H} site (Scheme 3, step v). This thermodynamically driven ET mechanism also suggests that superoxide channeling[9] is not a necessary event for the ET process, nor is the substrate mediated ET mechanism[8] because no change was observed in the EPR spectrum of resting PHM upon substrate binding, which indicates that the *J* value between the two Cu centers is still very small with substrate present.[22]

The noncoupled nature of the PHM and DβM active sites is very important for the chemistry catalyzed by these enzymes. If two Cu centers are strongly coupled, the O_2 reaction with the reduced protein leads to fast ET from both Cu sites to O_2, generating a 2-electron reduced binuclear or mononuclear peroxide-level species (O_2^{2-}), depending on the distance between the two Cu atoms, as summarized in Chart 1A−E. However, these Cu^{II}−peroxo/hydroperoxo complexes (Chart 1A−D) are not reactive in H−atom abstraction reaction,[4,55−60] nor is the mononuclear Cu^{II}_{M}−OOH species (Chart 1E) as shown in this study. Although 4-electron reduction of O_2 by two Cu atoms could lead to a bis-μ-oxo-Cu^{III}_2 species (Chart 1G), which is very reactive for H-atom abstraction, the existence of the Cu^{III} oxidation state in a biological environment is not known and most likely is not accessible due to the inability of biological ligands (histidines etc.) to stabilize the +3 oxidation state of copper. This is also the case for the mononuclear Cu^{III}−peroxide species (Chart 1F), which was synthesized recently with an exceptionally good electron-donating ligand (β-diketiminate).[61] Therefore, to form the 1-electron reduced superoxide-level species Cu^{II}_{M}−superoxo, which is reactive in H-atom abstraction (section 3.3), and not proceed further to 2-electron reduction, which is thermodynamically favored (section 4.1), the two Cu sites have to be noncoupled. This noncoupled nature of the binuclear active site provides a strategy for PHM and DβM to form a reactive Cu^{II}−superoxo species at one Cu site (Cu_M) for the required H-atom abstraction reactivity while maintaining the ability to provide an additional electron from another Cu site (Cu_H) to complete the reaction, where the intramolecular ET is switched on when there is enough driving force at the appropriate step in the enzymatic reaction.

Acknowledgment. This research has been supported by NIH Grant DK-31450 (E.I.S.). P.C. has been supported by a Gerhard Casper Stanford Graduate Fellowship and a Franklin Veatch Memorial Fellowship. We thank Drs. Betty Eipper and Joseph Bell for the collaborative spectroscopic studies in reference 22 which provided the structural basis for this study.

Supporting Information Available: Additional geometry optimized structures, tables of fragment charges of Cu^{II}_{M}−OOH and Cu^{II}_{M}−oxyl species, and molecular coordinates. This material is available free of charge via the Internet at http://www.acs.org. See any current masthead page for ordering information and Web access instructions.

JA031564G

(55) Kitajima, N.; Moro-oka, Y. *Chem. Rev.* **1994**, *94*, 737.
(56) Liang, H.-C.; Dahan, M.; Karlin, K. D. *Curr. Opin. Chem. Biol.* **1999**, *3*, 168.
(57) Decker, H.; Dillinger, R.; Tuczek, F. *Angew. Chem., Int. Ed.* **2000**, *39*, 1591.
(58) Schindler, S. *Eur. J. Inorg. Chem.* **2000**, 2311.
(59) Mahadevan, V.; Gebbink, R. J. M. K.; Stack, T. D. P. *Curr. Opin. Chem. Biol.* **2000**, *4*, 228.
(60) Que, L., Jr.; Tolman, W. B. *Angew. Chem., Int. Ed.* **2002**, *41*, 1114.
(61) Aboelella, N.; Lewis, E. A.; Reynolds, A. M.; Brennessei, W. W.; Cramer, C. J.; Tolman, W. B. *J. Am. Chem. Soc.* **2002**, *124*, 10660.